Monatsh Chem (2012) 143:1263–1274
DOI 10.1007/s00706-012-0772-y

ORIGINAL PAPER

Experimental investigation and thermodynamic modeling of the Au–Ge–Ni system

Shan Jin · Liliana I. Duarte · Guoxing Huang · Christian Leinenbach

Received: 18 February 2012 / Accepted: 15 April 2012

Abstract Phase equilibria in the Au–Ge–Ni ternary system were studied by means of scanning electron microscopy, electron probe microanalysis, X-ray diffraction, and differential scanning calorimetry. The phase relations in the solid state at 600 °C as well as a vertical section at $Au_{72}Ge_{28}$–Ni were established. No ternary compound was found at 600 °C. On the basis of the experimental phase equilibria data, a thermodynamic model of the Au–Ge–Ni ternary system was developed using the CALPHAD method. Thermodynamically calculated phase diagrams are shown at 600 °C, in two vertical sections and the liquidus projection. Reasonable agreement between the calculations and the experimental results was achieved.

Keywords Au–Ge–Ni · Thermodynamic · Phase diagram · CALPHAD

Dedicated to Professor Herbert Ipser on the occasion of his 65th birthday.

S. Jin · L. I. Duarte · C. Leinenbach (✉)
Laboratory for Joining Technologies and Corrosion, Empa, Swiss Federal Laboratories for Materials Science and Technology, Überlandstrasse 129, 8600 Dübendorf, Switzerland
e-mail: christian.leinenbach@empa.ch

S. Jin
Computational Materials Laboratory, Ecole Polytechnique Fédérale de Lausanne, Station 12, 1015 Lausanne, Switzerland

G. Huang
School of Material Science and Engineering, Central South University, Changsha 410083, Hunan, People's Republic of China

Introduction

High Pb content alloys which contain as much as 85 wt.% Pb have been widely used in the electronic and automotive industries as soldering materials for high temperature application. Given the potential environmental impact of Pb-based alloys, the development of high temperature Pb-free solders has become very urgent. Possible candidates are Zn-based alloys (Zn–Al, Zn–Sn) [1, 2], Bi-based alloys (Bi–Ag) [3], Sn–Sb based alloys [4], and especially Au-based alloys [5–8]. For example, Au–Si, Au–Sb, and Au–Ge alloy systems are all simple eutectic systems with low eutectic temperatures between 280 and 365 °C [9]. In addition to the low melting point, Au-based alloys also possess good thermal and electrical conductivity, excellent resistance to corrosion, high mechanical properties, etc. [10]. Among various Au-based alloys, Au–Ge-based alloys are very attractive as possible high temperature Pb-free solders because of their good wettability and high bonding strength with the substrate materials (e.g., Cu and Ni) [11, 12]. In order to better understand the interaction mechanism of the Au–Ge solders with the normally used substrate Ni to facilitate solder design and processing optimization, phase equilibria and thermodynamic properties of the Au–Ge–Ni system are indispensable.

Besides, Au–Ge or Au–Ge–Ni alloys have also been extensively used in ohmic contacts to GaAs semiconductors [13, 14]. Knowledge of the Au–Ge–Ni ternary system is also very important for their application in the semiconductor industry.

However, the available information on the Au–Ge–Ni ternary system is rather scarce. Jaffee and Gonser [15] studied the additions of Ni up to 12.2 at.% into the Au–Ge alloys by metallography, thermal analysis, and X-ray diffraction and reported that Ni has little effect on the Au–Ge

eutectic temperature. The freezing point of the eutectic line is lowered by Ni. In addition, they proposed that a ternary eutectic may occur in the Au–Ge–Ni ternary system. Christou [16] quoted a ternary eutectic temperature of 425 °C and stated that it was determined by a resistivity technique.

Therefore, the objectives of the present work were (1) to study the phase relations of the Au–Ge–Ni ternary system, including an isothermal section at 600 °C and a vertical section at $Au_{72}Ge_{28}$–Ni and liquidus projection; and (2) to develop the thermodynamic description of the Au–Ge–Ni ternary system using the CALPHAD (CALculation of PHAse Diagram) method [17].

Thermodynamic modeling

In the present optimization, the thermodynamic parameters of the Au–Ge, Au–Ni, and Ge–Ni binary subsystems are taken from [18], [19], and [20], respectively.

Pure elements

The pure elements in their stable structures at 298.15 K and 1 bar are chosen as the reference states for the system. The thermodynamic functions of the pure elements in their stable and metastable states are taken from the Scientific Group Thermodata Europe (SGTE) database [21] and are described as

$$ {}^{0}G_i^{\varphi}(T) - H_i^{\mathrm{SER}} = a + bT + cT\ln T + dT^2 + eT^3 + fT^{-1} + gT^7 + hT^{-9} \quad (1) $$

where H_i^{SER} is the molar enthalpy of the element i (i = Au, Ge, or Ni) at 298.15 K and 1 bar in its standard element reference (SER) state; T is the absolute temperature; $G_i^{\varphi}(T)$ is the absolute molar Gibbs energy of the element i with structure of φ; ${}^{0}G_i^{\varphi}(T)$ is the molar Gibbs energy of the element i with the structure of φ referred to the enthalpy of its stable state at 298.15 K and 1 bar.

Solution phases

The solution phase φ (φ = liquid, fcc, and diamond) is treated as a substitutional solution. Its molar Gibbs energy is expressed as

$$ G_{\mathrm{m}}^{\varphi} = x_{\mathrm{Au}}{}^{0}G_{\mathrm{Au}}^{\varphi} + x_{\mathrm{Ge}}{}^{0}G_{\mathrm{Ge}}^{\varphi} + x_{\mathrm{Ni}}{}^{0}G_{\mathrm{Ni}}^{\varphi} + RT(x_{\mathrm{Au}}\ln x_{\mathrm{Au}} + x_{\mathrm{Ge}}\ln x_{\mathrm{Ge}} + x_{\mathrm{Ni}}\ln x_{\mathrm{Ni}}) + {}^{\mathrm{E}}G_{\mathrm{m}}^{\varphi} + {}^{\mathrm{mag}}G_{\mathrm{m}}^{\varphi} \quad (2) $$

where G_{m}^{φ} is the molar Gibbs energy of a solution phase φ; ${}^{0}G_i^{\varphi}$ is the molar Gibbs energy of the element i (i = Au, Ge, or Ni) with the structure φ in a nonmagnetic state; x_i the mole fraction of component i, R gas constant, T temperature, ${}^{\mathrm{E}}G_{\mathrm{m}}^{\varphi}$ the excess Gibbs energy, and ${}^{\mathrm{mag}}G_{\mathrm{m}}^{\varphi}$ is the magnetic contribution to the Gibbs energy. The excess Gibbs energy of phase φ can be expressed by the Redlich–Kister polynomial [22] as

$$ {}^{\mathrm{E}}G_{\mathrm{m}}^{\varphi} = x_{\mathrm{Au}}x_{\mathrm{Ge}}L_{\mathrm{Au,Ge}}^{\varphi} + x_{\mathrm{Au}}x_{\mathrm{Ni}}L_{\mathrm{Au,Ni}}^{\varphi} + x_{\mathrm{Ge}}x_{\mathrm{Ni}}L_{\mathrm{Ge,Ni}}^{\varphi} + x_{\mathrm{Au}}x_{\mathrm{Ge}}x_{\mathrm{Ni}}L_{\mathrm{Au,Ge,Ni}}^{\varphi} \quad (3) $$

here $L_{\mathrm{Au,Ge}}^{\varphi}$, $L_{\mathrm{Au,Ni}}^{\varphi}$, and $L_{\mathrm{Ge,Ni}}^{\varphi}$ are the interaction parameters taken from the corresponding binary systems [18–20].

$$ L_{A,B}^{\varphi} = \sum_{j=0}^{n} {}^{(j)}L_{A,B}^{\varphi}(x_A - x_B)^j \quad (4) $$

where ${}^{(j)}L_{A,B}^{\varphi} = A_j + B_jT + C_jT\ln T$, and A_j, B_j, and C_j are model parameters evaluated from experimental information. $L_{\mathrm{Au,Ge,Ni}}^{\varphi}$ is the ternary interaction parameter with the following form:

$$ L_{\mathrm{Au,Ge,Ni}}^{\varphi} = x_{\mathrm{Au}}{}^{0}L_{\mathrm{Au,Ge,Ni}}^{\varphi} + x_{\mathrm{Ge}}{}^{1}L_{\mathrm{Au,Ge,Ni}}^{\varphi} + x_{\mathrm{Ni}}{}^{2}L_{\mathrm{Au,Ge,Ni}}^{\varphi} \quad (5) $$

where ${}^{i}L_{\mathrm{Au,Ge,Ni}}^{\varphi} = a_i + b_iT$, and a_i and b_i are model parameters to be evaluated in the present optimization.

Intermetallic compounds

There are no intermetallic compounds in the Au–Ge and Au–Ni binary systems. In the Ge–Ni binary system, βNi_3Ge phase has the ordered variant of the disordered fcc structure ($L1_2$ type). Hence, it was modeled as (Au,Ge,Ni)$_{0.75}$(Au,Ge,Ni)$_{0.25}$ in the Au–Ge–Ni ternary system. The parameters which were introduced by employing Au into the sublattice were given as zero because neither experimental nor theoretical thermodynamic data for those metastable end members are available. According to the present experimental results, the solubility of the element Au in the binary Ge–Ni intermetallic compounds is fairly small. Therefore, the Gibbs energies of all the other binary Ge–Ni intermetallic compounds were taken directly from Ref. [20].

Results and discussion

Experimental results

All prepared and investigated samples are listed in Tables 1 and 2. The microstructures of the samples after heat treatment at 600 °C are shown in Fig. 1. The phase compositions were determined by electron probe microanalysis (EPMA). A two-phase equilibrium between fcc(Au) and Ni_5Ge_3 was observed in alloys 5, 13, and 14 (Table 2). Figure 1a shows the backscattered electron (BSE) image of annealed sample 5. The compositions of

Table 1 Nominal compositions of the Au–Ge–Ni alloys produced by arc-melting, primary phases observed on solidification, phase transformation temperatures measured by DSC during heating

Alloy number	Nominal composition/at.%			Primary phase	DSC signals on heating/°C							
	Au	Ge	Ni		5 °C/min				10 °C/min			
1	71.3	27.7	1.0	NiGe	364[a]	378		386[b]	362[a]	375		383[b]
2	68.4	26.6	5.0	NiGe	363[a]	464		620[b]	362[a]			625[b]
3	64.1	24.9	11	Ni_5Ge_3	364[a]	550[a]	559[c]	807[b]	362[a]	548[a]		804[b]
4	60	23	17	Ni_5Ge_3	363[a]	551[a]	650[c]	878[b]	362[a]	546[a]	651[c]	882[b]
5	50.4	19.6	30	Ni_5Ge_3	611	832		974[b]	610	828		970[b]
6	41.8	16.2	42	βNi_3Ge	904[a]			978[b]	904[a]			976[b]
7	36	14	50	βNi_3Ge	931	935[c]		1,008[b]	930	937[c]		1,003[b]
8	28.8	11.2	60	βNi_3Ge	922[a]			1,040[b]	921[a]			1,042[b]
9	25.2	9.8	65	fcc(Ni)	922[a]	929[c]		1,121[b]	920[a]	930[c]		1,122[b]
10	21.6	8.4	70	fcc(Ni)	922[a]	924[c]	931[c]	1,156[b]	921[a]	924[c]	933[c]	1,161[b]
11	14.4	5.6	80	fcc(Ni)	941[a]			1,278[b]	941[a]			1,275[b]
12	7.2	2.8	90	fcc(Ni)	–	–	–	–		1,189		
13	74	10.3	15.7	fcc(Au)	871				869			910[b]
14	68.9	12.3	18.8	Ni_5Ge_3				896[b]				899[b]
15	61	3.2	35.8	fcc(Au)	922[a]			944[b]	919[a]			937[b]
16	10	80	10	(Ge)	362[a]	716		854[b]	362[a]	718		855[b]
17	20	60	20	NiGe	363[a]	702		752[b]	362[a]	706		754[b]

DSC differential scanning calorimetry, – experiment not performed

[a] Invariant reaction

[b] Liquidus temperature

[c] Weak signal

the dark phase and the white phase as measured by EPMA are 38.7 at.% Ge–61.3 at.% Ni and 97.6 at.% Au–2.4 at.% Ni, corresponding to the Ni_5Ge_3 and fcc(Au) phases, respectively. The solubility of Au in the Ni_5Ge_3 phase is almost zero. The microstructure of alloy 6 after heat treatment at 600 °C for 1,464 h is shown in Fig. 1b. The white phase and the big dark phase were identified by EPMA as fcc(Au) and βNi_3Ge, respectively. The small round gray phase is too small to be precisely identified by EPMA. A two-phase microstructure fcc(Au) + βNi_3Ge was found in alloys 7 and 8 according to their compositions measured by EPMA. Figure 1c presents the scanning electron microscopy (SEM) image of annealed alloy 8. Alloy samples 9, 10, 11, and 12 show a two-phase equilibrium between fcc(Au) and fcc(Ni). As an example, the microstructure of annealed alloy 11 is presented in Fig. 1d. Table 2 lists the compositions of the coexisting phases measured by EPMA on the samples annealed at 600 °C. No solubility of Au was detected in the Ni_5Ge_3 phase and the solubility of Au in βNi_3Ge is less than 4 at.%. The solubilities of Ni in fcc(Au) range from 1 to 5 at.% in alloy samples 5, 6, 13, and 14, whereas larger amounts of Ni, from 14 up to 25 at.%, are dissolved in fcc(Au) in samples 7, 8, 9, 10, 11, and 12.

To further confirm the phase constitution, XRD was performed on alloy samples 6, 7, 8, and 10. A three-phase equilibrium, fcc(Au), βNi_3Ge, and Ni_5Ge_3, was confirmed in annealed alloy 6. The diffraction pattern of the annealed alloy 6 is illustrated in Fig. 2a. Combining with the EPMA results, the small round gray phase presented in the annealed microstructure of alloy 6 (Fig. 1b) is the Ni_5Ge_3 phase. Two phases, fcc(Au) and βNi_3Ge, were detected in alloy samples 7 and 8. Figure 2b presents the diffraction pattern of the annealed alloy 8. The two-phase equilibrium, fcc(Au) and fcc(Ni), was identified in the annealed alloy 10.

DSC measurements were carried out on samples that had been annealed at 325 °C for 648 h. Temperatures of thermal effects which were found in both heating cycles were in good agreement with each other. As significant supercooling was noticed in the recorded cooling curves, relevant phase diagram information was taken from the heating curve. Table 1 summarizes the results of the thermal analysis from the first heating curve for 10 and 5 °C/min scanning rates. For illustration, Fig. 3 depicts heating curves obtained by DSC for selected alloy samples.

The microstructures of the as-cast alloys and the alloys after DSC measurements (scanning rate 10 °C/min) were

Table 2 Summary of the phase compositions measured by EPMA for the Au–Ge–Ni ternary alloys annealed at 600 °C

Alloy number	Annealing time/h	EPMA results/at.%			Phase identified	Technique
		Au	Ge	Ni		
5	720	0	38.7	61.3	Ni_5Ge_3	EPMA
		97.6	0	2.4	fcc(Au)	EPMA
6	1,464	3.3	23.7	73	βNi_3Ge	EPMA + XRD
		94.7	0	5.3	fcc(Au)	EPMA + XRD
		ND	ND	ND	Ni_5Ge_3	XRD
7	1,464	1.1	24	74.9	βNi_3Ge	EPMA + XRD
		86.3	0	13.7	fcc(Au)	EPMA + XRD
8	1,464	4	21	75	βNi_3Ge	EPMA + XRD
		84	0	16	fcc(Au)	EPMA + XRD
9	1,464	4.6	11.4	84	fcc(Ni)	EPMA
		79	0	21	fcc(Au)	EPMA
10	1,464	5.1	9.4	85.6	fcc(Ni)	EPMA + XRD
		79	0	21	fcc(Au)	EPMA + XRD
11	1,464	5.2	6.1	88.7	fcc(Ni)	EPMA
		76	0	24	fcc(Au)	EPMA
12	1,464	3.3	2.6	94	fcc(Ni)	EPMA
		75	0	25	fcc(Au)	EPMA
13	720	0	38.1	61.9	Ni_5Ge_3	EPMA
		95	0	5	fcc(Au)	EPMA
14	1,464	0	38.7	61.3	Ni_5Ge_3	EPMA
		98.8	0	1.2	fcc(Au)	EPMA

ND not possible to determine, *XRD* X-ray diffraction

characterized by SEM, as shown in Figs. 4 and 5. Figure 4a illustrates the microstructure of the as-cast sample 1. Three phases, fcc(Au), NiGe, and (Ge), were observed, with NiGe as the primary phase. The primary solidification of the Ni_5Ge_3 phase is observed in alloys 3, 4, 5, and 14, as shown in Fig. 4b (alloy 3). The βNi_3Ge phase was found as the primary phase in samples 6, 7, and 8 (Fig. 4c, as-cast alloy 6; Fig. 4d, as-cast alloy 8). The fcc(Ni) phase was the primary phase in as-cast samples 9, 10, 11, and 12, whereas fcc(Au) was the primary phase in samples 13 and 15. Figure 5a, b shows the microstructures of samples 16 and 17 after DSC measurements with the scanning rate of 10 °C/min. As can been seen, a three-phase microstructure fcc(Au), (Ge), and NiGe was observed in both samples. However, they show different solidification sequences. The (Ge) phase is the primary phase in sample 16 whereas NiGe crystallized first from the liquid in sample 17. Table 1 compiles the primary phases observed in all the alloy samples.

Thermodynamic assessment

Combining the previous assessments of the Au–Ge [18], Au–Ni [19], and Ge–Ni [20] binary systems, we optimized the Au–Ge–Ni ternary system on the basis of the experimental data obtained in the present work. The optimization of the model parameters for various phases in the Au–Ge–Ni ternary system was conducted using the PARROT module [23] in the Thermo-calc software package developed by Sundman et al. [24]. The thermodynamic parameters for all condensed phases in the Au–Ge–Ni ternary system obtained in the present work together with the thermodynamic parameters of the three binary systems Au–Ge, Au–Ni, and Ge–Ni from literature [18–20] are summarized in Table 3.

Figure 6 shows the calculated isothermal section at 600 °C. Tie-lines determined by EPMA in the present work were superimposed for comparison. The three-phase field fcc(Au) + Ni_5Ge_3 + βNi_3Ge and two-phase fields fcc(Au) + Ni_5Ge_3, fcc(Au) + βNi_3Ge, fcc(Au) + fcc(Ni) are well reproduced. However, the nominal composition of alloy 8 lies in a three-phase field fcc(Au) + βNi_3Ge + fcc(Ni) according to the calculation, whereas only two phases fcc(Au) and βNi_3Ge were identified in the annealed sample. It should be noted that similar morphologies were observed for the as-cast state and after annealing, as can been seen from Figs. 1c and 4d. This implies that full equilibrium has possibly not been obtained in alloy 8. Besides, the calculated solubilities of Au and Ge in fcc(Ni) are lower than the measured values. The difference may be due to full equilibrium not being achieved in alloys 9, 10, 11, 12 even after 1,462 h of annealing. This can be seen from the BSE image of annealed alloy 11 (Fig. 1d) in which the fcc(Ni) phase appears in different

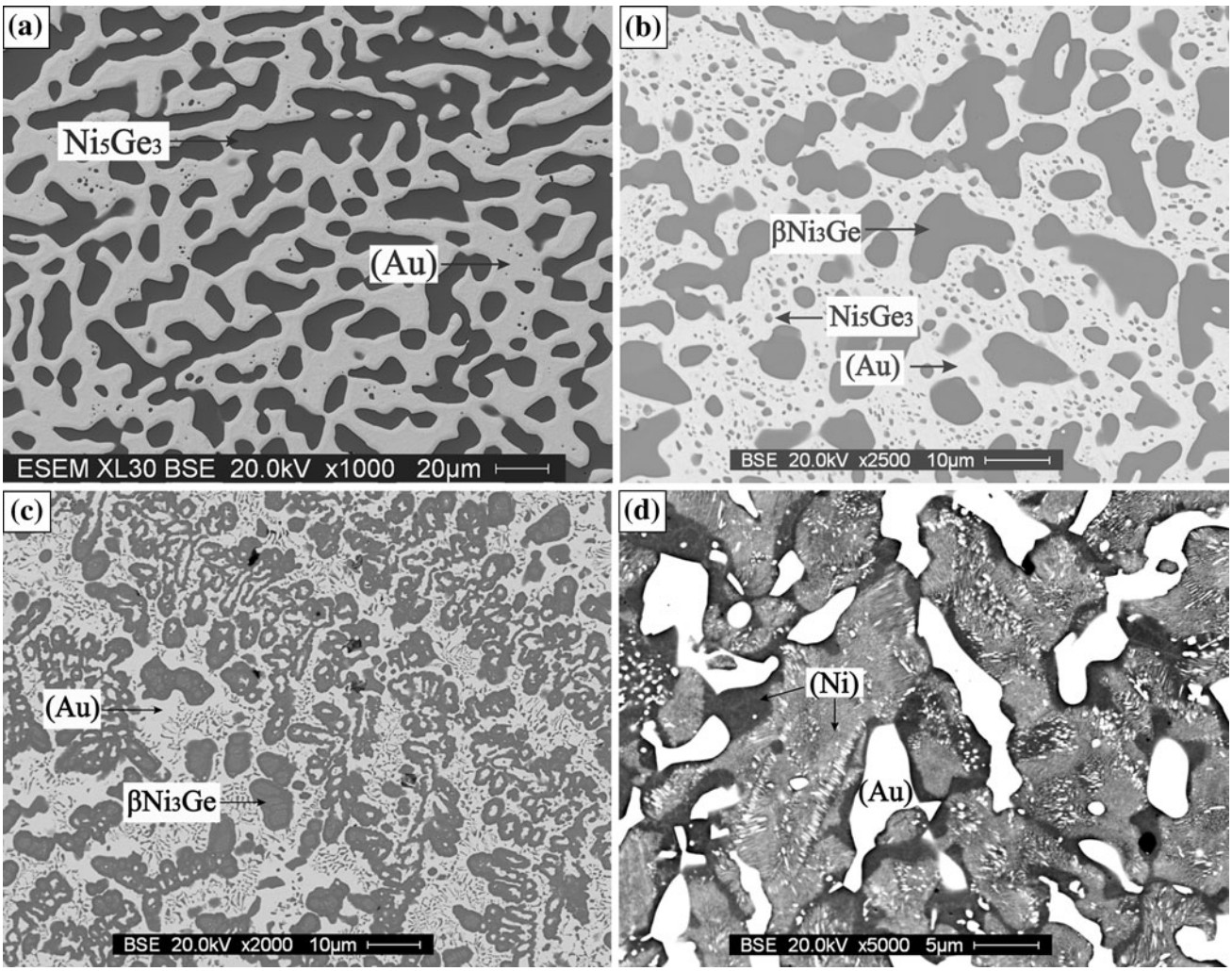

Fig. 1 BSE images of the Au–Ge–Ni alloy samples annealed at 600 °C. **a** Alloy 5: Au–19.6 at.% Ge–30 at.% Ni, **b** alloy 6: Au–16.24 at.% Ge–42 at.% Ni, **c** alloy 8: Au–11.2 at.% Ge–60 at.% Ni, **d** alloy 11: Au–5.6 at.% Ge–80 at.% Ni

contrasts, which means that interdiffusion of the elements is still going on.

The calculated vertical section $Au_{72}Ge_{28}$–Ni compared with the experimental data obtained in the present work is shown in Fig. 7. Good agreement between calculation and experiment was obtained. The liquidus and most of the phase transformations were well reproduced. However, there are some deviations for alloy 1. Three thermal signals were observed in alloy 1. The first thermal effect was measured at $T = 363$ °C (the average value of the data at 5 and 10 °C/min), agreeing well with the calculated value 357 °C. The second thermal effect happened at $T = 378$ °C while the calculated temperature is 406 °C. The difference originates from the deviation of the calculated eutectic composition from the experiment in the Au–Ge binary system. The investigated vertical section in this work starts from the Au–Ge experimental eutectic point (28 at.% Ge) to pure Ni. However, the calculated Au–Ge eutectic composition is at 29.5 at.% Ge [18], which leads to the higher calculated transition temperature for the Au–Ge–Ni ternary alloy 1. The calculated liquidus temperature (ca. 460 °C) for alloy 1 is also higher than the corresponding experimental value (386 °C). If the liquidus temperatures of alloy 1 and all the other alloys were reproduced at the same time, the liquidus would have to be much steeper in a very narrow composition range, from 0 to 4 at.% Ni, which is unreasonable. Hence, the measured liquidus temperature of alloy 1 might have large experimental uncertainty, which may arise from the inhomogeneity of the sample.

Besides, the thermal signals for the phase transformations at low temperature in alloy 6, 7, 8, and 9 were not observed or were too weak to be analyzed. It should be noted that there is no liquid phase involved in those reactions. The liquidus temperature of alloy 12 was not reached because the maximum measuring temperature was 1,300 °C.

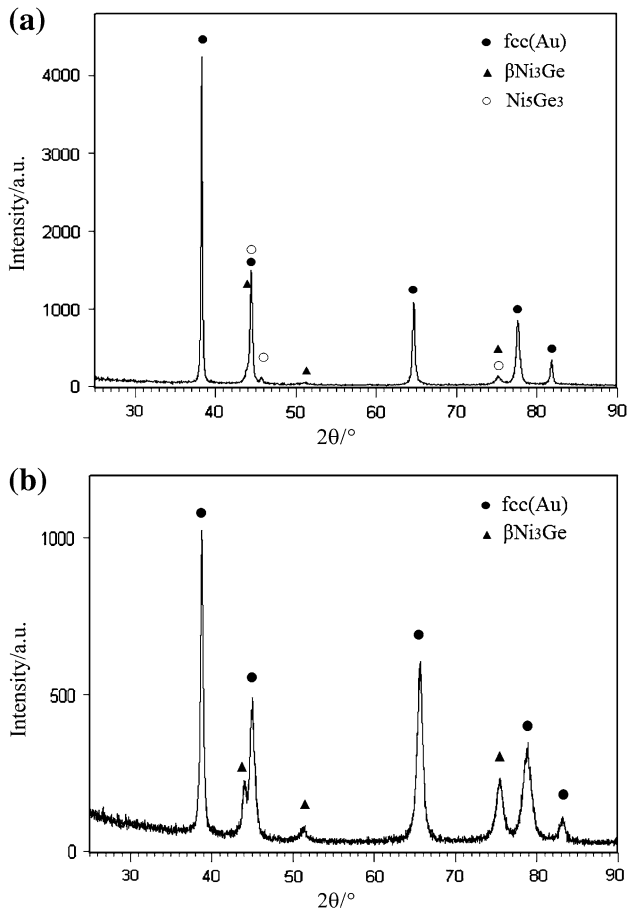

Fig. 2 Diffraction patterns of the samples after heat treatment at 600 °C. **a** Alloy 6: Au–16.24 at.% Ge–42 at.% Ni, **b** alloy 8: Au–11.2 at.% Ge–60 at.% Ni

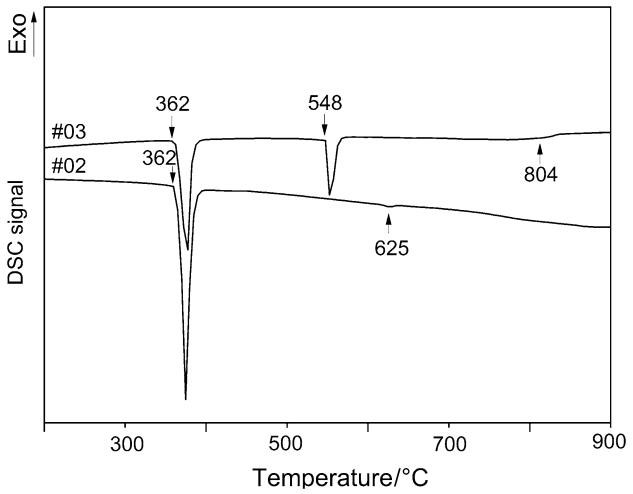

Fig. 3 DSC curves recorded upon heating with a rate of 10 °C/min for selected samples

Figure 8 shows the calculated vertical section at Ge–$Au_{50}Ni_{50}$ compared with the experimental data obtained in the present work. As can be seen, good agreement was obtained.

The calculated liquidus projection of the Au–Ge–Ni ternary system superimposed with the experimentally determined primary phases is presented in Fig. 9. The regions of primary crystallized phases observed in the present work are generally well reproduced in the present calculation, but some discrepancies were found in alloys 2, 8, and 14. It should be noted that the nominal compositions of those alloys are very close to the monovariant line.

Table 4 summarizes the types and temperatures of the invariant reactions together with the compositions of the participating liquid phases. The invariant reactions U_1 ($L + \gamma Ni_3Ge \leftrightarrow \beta Ni_3Ge + \delta Ni_5Ge_2$) and U_2 ($L + \delta Ni_5Ge_2 \leftrightarrow Ni_5Ge_3 + \beta Ni_3Ge$) were not investigated experimentally in the present work due to the too small primary crystallization fields of γNi_3Ge and δNi_5Ge_2. An interesting ternary quasi-peritectic U_3 ($L + fcc \leftrightarrow fcc + \beta Ni_3Ge$) at 937 °C is predicted by the present calculation. The existence of this ternary quasi-peritectic invariant reaction (U_3) was proved by the experimental results. As can be seen from Table 1, a ternary invariant reaction which happens at 921 °C was observed in alloys 8, 9, 10, and 15. The ternary eutectic reaction E_1 ($L \leftrightarrow Ge + NiGe + fcc$) and ternary quasi-peritectic reaction U_4 ($L + \beta Ni_3Ge \leftrightarrow fcc + Ni_5Ge_3$) are well reproduced, with only a temperature difference of 5 and 15 °C between calculation and experiment, respectively. However, for the reaction U_5 ($L + Ni_5Ge_3 \leftrightarrow NiGe + fcc$), the calculated invariant temperature is 497 °C, 52 °C lower than the corresponding experimental value (549 °C). This difference is caused by the thermodynamic parameters of the NiGe phase in the Ge–Ni binary system. The temperature difference could be shortened and meanwhile the nominal composition of alloy 2 would fall into the NiGe primary crystallization field if a more exothermic enthalpy of formation for the NiGe phase was given. However, the reaction type of the binary invariant reaction $Ni_5Ge_3 \leftrightarrow \varepsilon' Ni_5Ge_3 + NiGe$ will be changed from eutectoid to peritectoid ($Ni_5Ge_3 + NiGe \leftrightarrow \varepsilon' Ni_5Ge_3$) in the Ge–Ni binary system. Besides, a temperature difference of 50 °C is considered to be still acceptable for this ternary system. Therefore, the thermodynamic parameters of the NiGe phase are kept the same as the one from the binary system [20].

The ternary eutectic temperature of 425 °C which was quoted by Christou [16] was not found in the present work. However, Christou [16] only mentioned that it was determined by a resistivity technique. No further details were given in his work.

A detailed overview over the nature and sequence of these ternary invariant reactions and their connections to the binary boundary systems is given by the calculated reaction scheme (Scheil diagram) shown in Fig. 10.

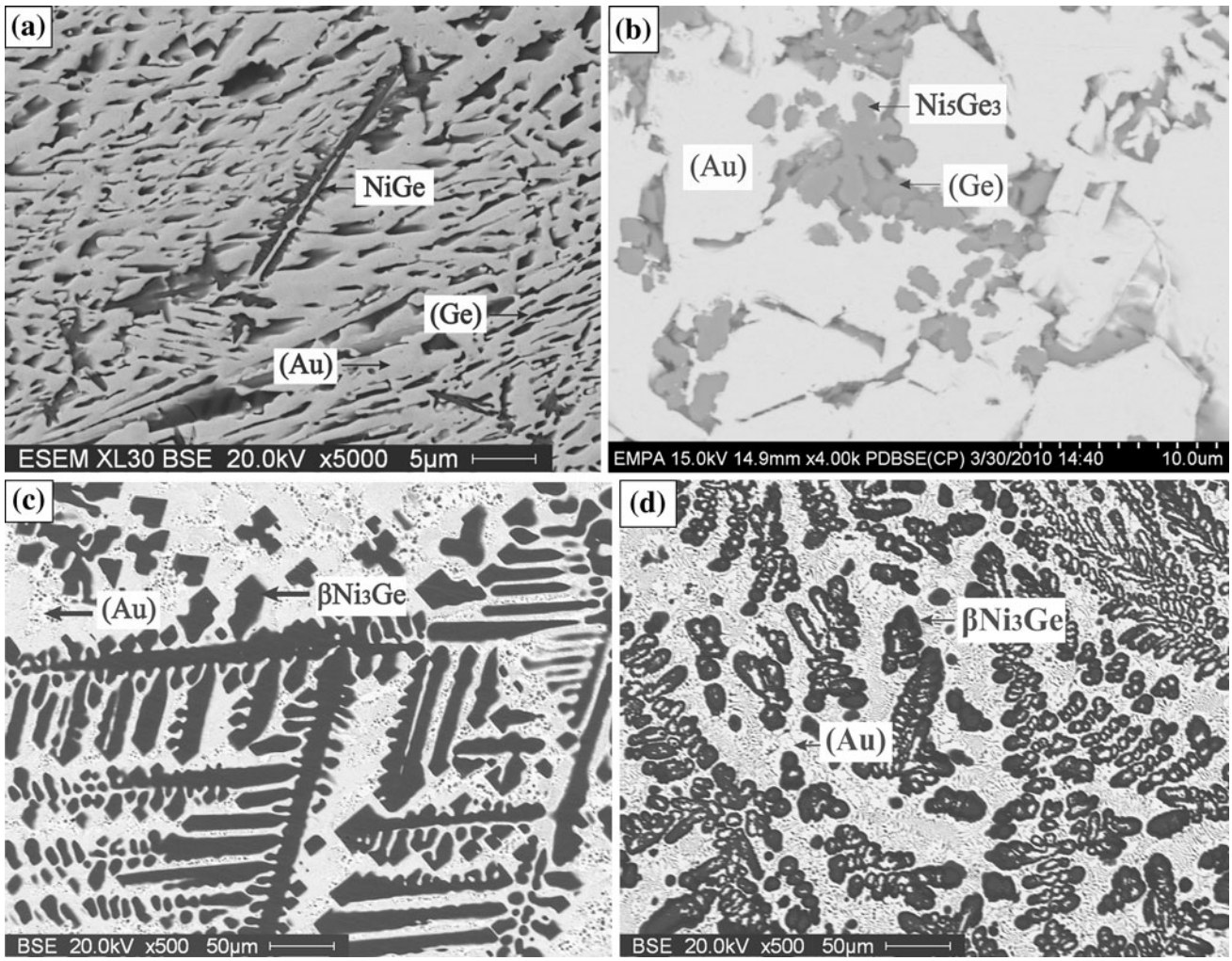

Fig. 4 As-cast microstructures of **a** alloy 1: Au–27.72 at.% Ge–1 at.% Ni, **b** alloy 3: Au–24.92 at.% Ge–11 at.% Ni, **c** alloy 6: Au–16.24 at.% Ge–42 at.% Ni, **d** alloy 8: Au–11.2 at.% Ge–60 at.% Ni

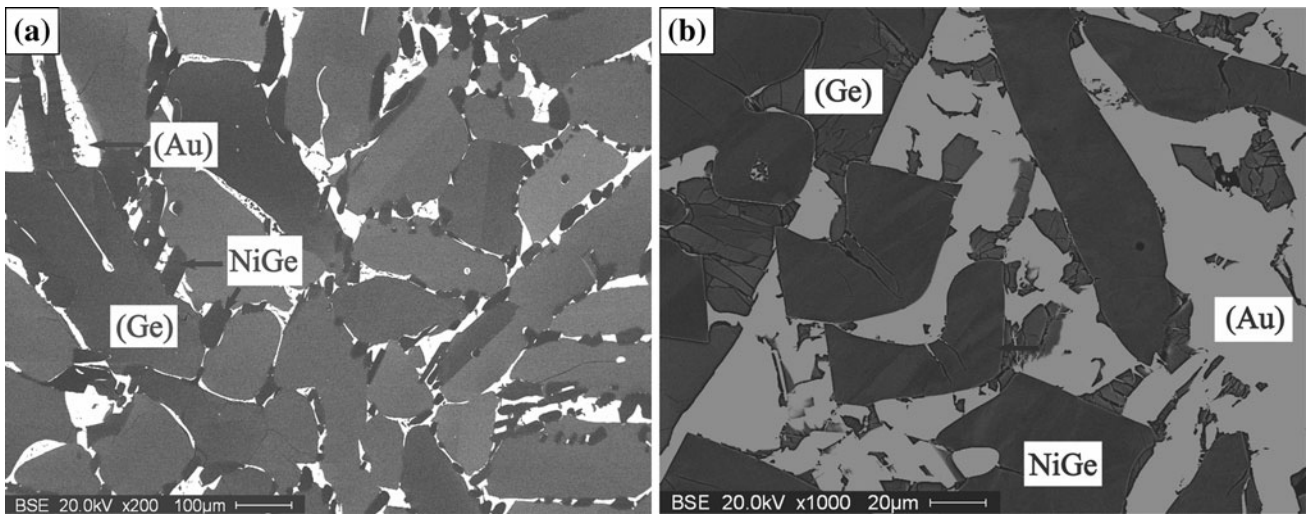

Fig. 5 Microstructures of the samples after DSC measurement (scanning rate 10 °C/min). **a** Alloy 16: Au–80 at.% Ge–10 at.% Ni, **b** alloy 17: Au–60 at.% Ge–20 at.% Ni

Table 3 Thermodynamic parameters of the Au–Ge–Ni ternary system

	References
Liquid (Au,Ge,Ni)	
${}^{0}L^{\text{liquid}}_{\text{Au,Ge}} = -18,294.684 - 13.671T$	[18]
${}^{1}L^{\text{liquid}}_{\text{Au,Ge}} = -8,894.639 - 6.339T$	[18]
${}^{2}L^{\text{liquid}}_{\text{Au,Ge}} = -2,174.476 - 4.925T$	[18]
${}^{0}L^{\text{liquid}}_{\text{Au,Ni}} = 9,500 - 5.429T$	[19]
${}^{1}L^{\text{liquid}}_{\text{Au,Ni}} = 1,614$	[19]
${}^{0}L^{\text{liquid}}_{\text{Ge,Ni}} = -167,121.320 + 155T - 15T\ln T$	[20]
${}^{1}L^{\text{liquid}}_{\text{Ge,Ni}} = 84,737.489 - 25.014T$	[20]
${}^{2}L^{\text{liquid}}_{\text{Ge,Ni}} = 37,441.590 - 16.001T$	[20]
${}^{3}L^{\text{liquid}}_{\text{Ge,Ni}} = -63,650.323 + 21.983T$	[20]
${}^{0}L^{\text{liquid}}_{\text{Au,Ge,Ni}} = -140,000$	This work
fcc: (Au,Ge,Ni)	
${}^{0}L^{\text{fcc}}_{\text{Au,Ge}} = 10,198.859 - 23.114T$	[18]
${}^{0}L^{\text{fcc}}_{\text{Au,Ni}} = 28,696 - 11.274T$	[19]
${}^{1}L^{\text{fcc}}_{\text{Au,Ni}} = -10,945 + 6.154T$	[19]
${}^{2}L^{\text{fcc}}_{\text{Au,Ni}} = 2,519$	[19]
${}^{0}L^{\text{fcc}}_{\text{Ge,Ni}} = -122,000 + 36.88T$	[20]
${}^{1}L^{\text{fcc}}_{\text{Ge,Ni}} = 134,000 - 46.8T$	[20]
${}^{0}Tc^{\text{fcc}}_{\text{Ge,Ni}} = -3,750$	[20]
${}^{0}L^{\text{fcc}}_{\text{Au,Ge,Ni}} = -320,000$	This work
${}^{1}L^{\text{fcc}}_{\text{Au,Ge,Ni}} = 0$	This work
${}^{2}L^{\text{fcc}}_{\text{Au,Ge,Ni}} = 91,000$	This work
βNi_3Ge: $(Ge,Ni)_{0.75}(Ge,Ni)_{0.25}$	
${}^{0}G^{\beta\text{Ni}_3\text{Ge}}_{\text{Ge:Ni}} - 0.75{}^{0}G^{\text{diamond}}_{\text{Ge}} - 0.25{}^{0}G^{\text{fcc}}_{\text{Ni}} = -46,827.192 + 3.05T$	[20]
${}^{0}G^{\beta\text{Ni}_3\text{Ge}}_{\text{Ni:Ge}} - 0.25{}^{0}G^{\text{diamond}}_{\text{Ge}} - 0.75{}^{0}G^{\text{fcc}}_{\text{Ni}} = -46,827.192 + 3.05T$	[20]
${}^{0}G^{\beta\text{Ni}_3\text{Ge}}_{\text{Ge:Ge}} - {}^{0}G^{\text{diamond}}_{\text{Ge}} = 0$	[20]
${}^{0}G^{\beta\text{Ni}_3\text{Ge}}_{\text{Ni:Ni}} - {}^{0}G^{\text{fcc}}_{\text{Ni}} = 0$	[20]
${}^{0}L^{\beta\text{Ni}_3\text{Ge}}_{\text{Ge,Ni:Ge}} = -93,654.384 + 6.1T$	[20]
${}^{0}L^{\beta\text{Ni}_3\text{Ge}}_{\text{Ge,Ni:Ni}} = -93,654.384 + 6.1T$	[20]
${}^{1}L^{\beta\text{Ni}_3\text{Ge}}_{\text{Ge,Ni:Ge}} = 23,700 - 9.72T$	[20]
${}^{1}L^{\beta\text{Ni}_3\text{Ge}}_{\text{Ge,Ni:Ni}} = 23,700 - 9.72T$	[20]
${}^{0}L^{\beta\text{Ni}_3\text{Ge}}_{\text{Ni:Ge,Ni}} = 0$	[20]
${}^{0}L^{\beta\text{Ni}_3\text{Ge}}_{\text{Ni:GeGe}} = 0$	[20]
${}^{1}L^{\beta\text{Ni}_3\text{Ge}}_{\text{Ni:Ge,Ni}} = 7,900 - 3.24T$	[20]
${}^{1}L^{\beta\text{Ni}_3\text{Ge}}_{\text{Ge:Ge,Ni}} = 7,900 - 3.24T$	[20]
γNi_3Ge: $(Ge)_{0.256}(Ni)_{0.744}$	
${}^{0}G^{\gamma\text{Ni}_3\text{Ge}}_{\text{Ni:Ge}} - 0.256{}^{0}G^{\text{diamond}}_{\text{Ge}} - 0.744{}^{0}G^{\text{fcc}}_{\text{Ni}} = -34,315 + 4.301T$	[20]
δNi_5Ge_2: $(Ge)_{0.28}(Ni)_{0.72}$	
${}^{0}G^{\delta\text{Ni}_5\text{Ge}_2}_{\text{Ni:Ge}} - 0.28{}^{0}G^{\text{diamond}}_{\text{Ge}} - 0.72{}^{0}G^{\text{fcc}}_{\text{Ni}} = -34,918 + 3.69T$	[20]
Ni_2Ge: $(Ge)_{0.335}(Ni)_{0.665}$	
${}^{0}G^{\text{Ni}_2\text{Ge}}_{\text{Ni:Ge}} - 0.335{}^{0}G^{\text{diamond}}_{\text{Ge}} - 0.665{}^{0}G^{\text{fcc}}_{\text{Ni}} = -38,227.151 + 4.849T$	[20]
Ni_5Ge_3: (Ge)(Ni)(Va,Ni)	
${}^{0}G^{\text{Ni}_5\text{Ge}_3}_{\text{Ge:Ni:Va}} - {}^{0}G^{\text{diamond}}_{\text{Ge}} - {}^{0}G^{\text{fcc}}_{\text{Ni}} = -54,286.304 - 5.624T$	[20]
${}^{0}G^{\text{Ni}_5\text{Ge}_3}_{\text{Ge:Ni:Ni}} - {}^{0}G^{\text{diamond}}_{\text{Ge}} - 2{}^{0}G^{\text{fcc}}_{\text{Ni}} = -110,540 + 11.717T$	[20]
${}^{0}L^{\text{Ni}_5\text{Ge}_3}_{\text{Ge:Ni:Ni,Va}} = -2,655.913 - 2.932T$	[20]
${}^{1}L^{\text{Ni}_5\text{Ge}_3}_{\text{Ge:Ni:Ni,Va}} = -17,558.144$	[20]
ε'Ni_5Ge_3: $(Ge)_{0.375}(Ni)_{0.625}$	
${}^{0}G^{\varepsilon'\text{Ni}_5\text{Ge}_3}_{\text{Ni:Ge}} - 0.375{}^{0}G^{\text{diamond}}_{\text{Ge}} - 0.625{}^{0}G^{\text{fcc}}_{\text{Ni}} = -37,350.646 + 3.328T$	[20]
NiGe: $(Ge)_{0.5}(Ni)_{0.5}$	
${}^{0}G^{\text{NiGe}}_{\text{Ni:Ge}} - 0.5{}^{0}G^{\text{diamond}}_{\text{Ge}} - 0.5{}^{0}G^{\text{fcc}}_{\text{Ni}} = -30,992.547 + 0.967T - 0.1T\ln T + 6.015E-05T^2 - 9.471E-08T^3 + 2.393E-22T^7 - 14,960.491T^{-1}$	[20]

Gibbs energies are expressed in J/mol. The lattice stabilities were given by Dinsdale [21]

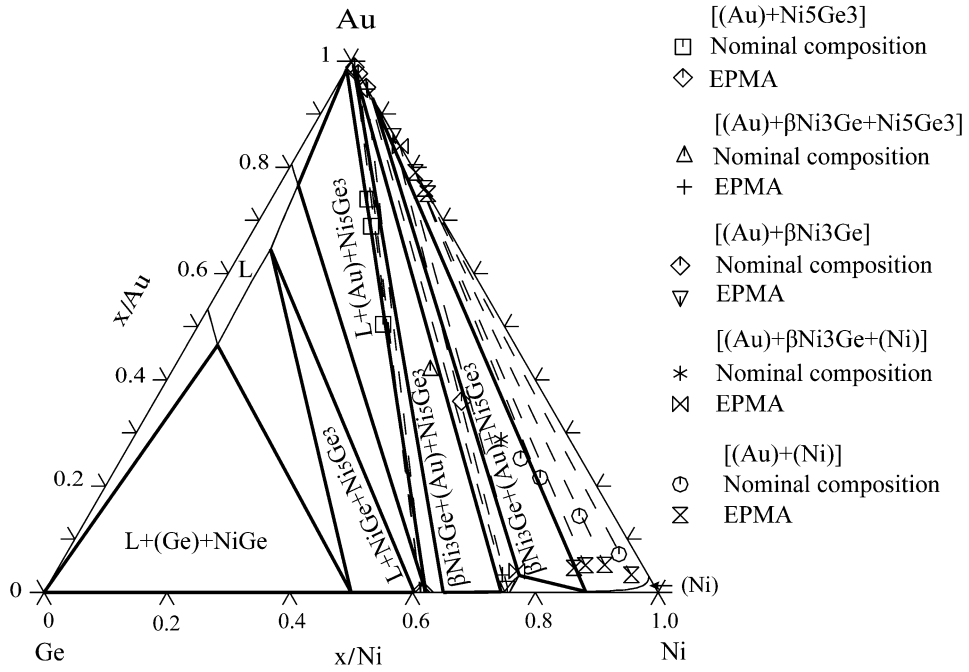

Fig. 6 Calculated isothermal section at 600 °C compared with the experimental data measured in the present work

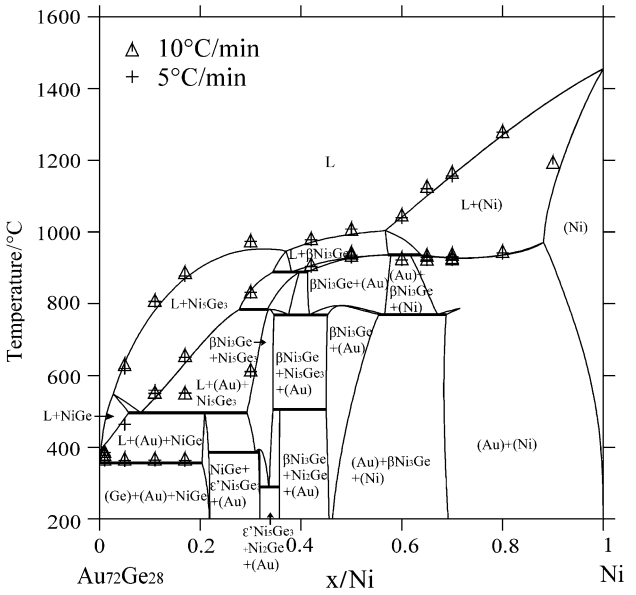

Fig. 7 Calculated vertical section at $Au_{72}Ge_{28}$–Ni compared with the experimental data in the present work

Conclusions

Phase equilibria in the Au–Ge–Ni ternary system were experimentally studied and a full thermodynamic description was established. A vertical section at $Au_{72}Ge_{28}$–Ni and a partial isothermal section at 600 °C were experimentally determined. The solubility of Au in the Ni_5Ge_3 phase is less than 4 at.% and no solubility of Au was observed in the βNi_3Ge phase. No ternary compound was found at 600 °C. The calculated liquidus projection reproduces the experimental data well. Five ternary quasi-peritectic reactions and one ternary eutectic reaction were proposed. The reasonable agreement between the thermodynamic calculations and the experimental results supports the reliability of the present thermodynamic modeling of the Au–Ge–Ni ternary system. These results provide important information for developing and designing Au–Ge-based alloys as high-temperature lead-free solders.

Experiments

Seventeen samples with different composition were produced. All alloy compositions are listed in Table 1. The starting materials were pure elements of Au wire (99.99 %), Ge pieces (99.999 %), and Ni slug and wire (99.98 %) supplied by Alfa Aesar GmbH, Germany.

Alloys of 1 g were produced by arc-melting under high-purity argon atmosphere (Ar 6.0) using a non-consumable tungsten electrode. All alloys were melted five times and inverted after three meltings to ensure homogeneity. In order to have a clean atmosphere during the melting, a Ti alloy was melted first as an oxygen getter. In addition, an oxygen cartridge in the argon line was used. No chemical analysis of the alloys was conducted because the weight losses during melting were less than 0.3 mass% in all cases.

Afterwards, the samples were cut into three pieces for different purposes. One was used to investigate the as-cast

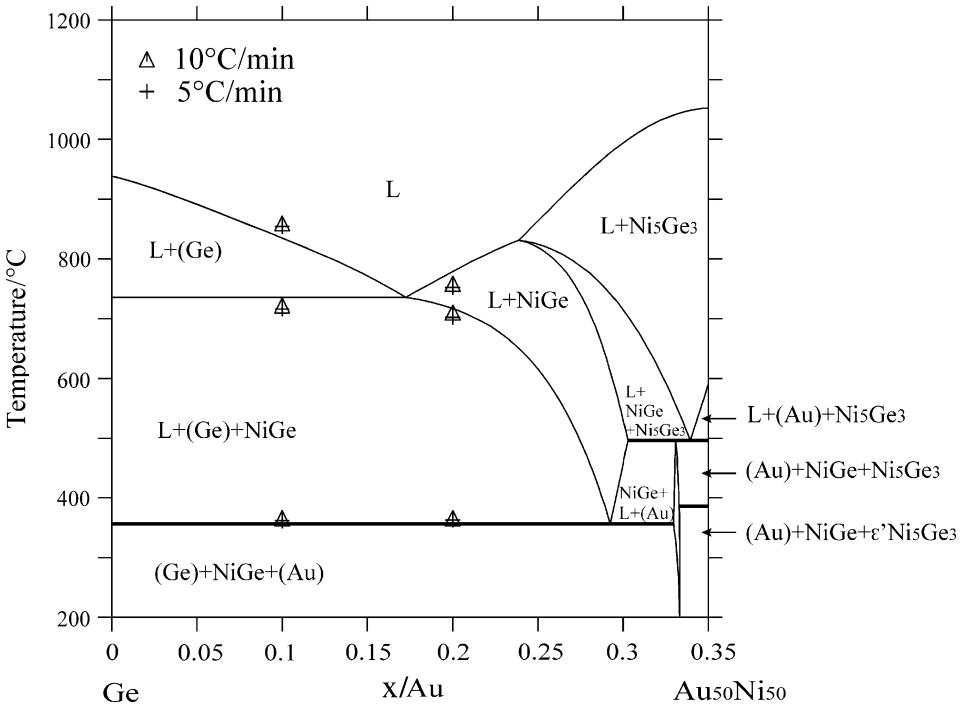

Fig. 8 Calculated vertical section at Ge–$Au_{50}Ni_{50}$ compared with the experimental data in the present work

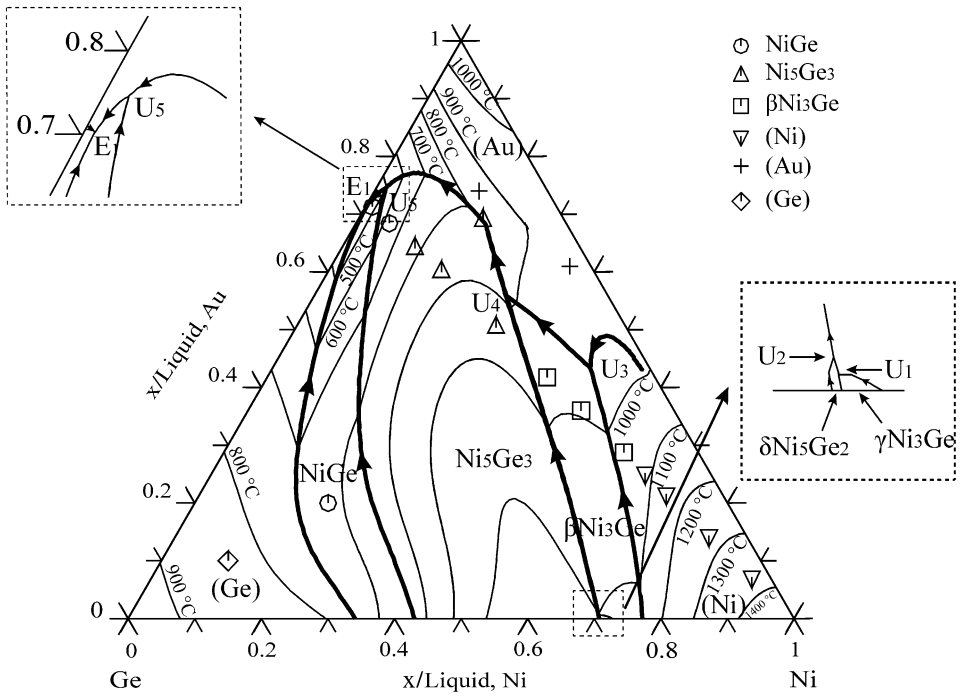

Fig. 9 Calculated liquidus projection of the Au–Ge–Ni ternary system superimposed with the experimental data of primary solidification

microstructure; another one was used for DSC measurements after homogenization heat treatment at 325 °C for 648 h; and one was used to investigate the microstructure after annealing experiments at 600 °C. For the heat treatments the samples were placed in evacuated quartz tubes refilled with argon. Before the encapsulation the samples were cleaned in acetone, dried, and wrapped in tantalum foil to avoid reactions with the quartz tube. The annealing experiments were performed at 600 °C for 720–1,464 h in an electric resistance furnace with a temperature accuracy of ±3 °C. After annealing, the samples were quenched in salt water to retain the equilibrium microstructures.

Phase transitions and thermal reactions were determined by DSC performed on a Netzsch DSC 404 F3 Pegasus, using open alumina crucibles. The DSC cells were calibrated using the melting temperatures of the pure elements

Table 4 Calculated ternary invariant reactions involving liquid phase with the experimental data

Invariant reaction	Type	T/°C		Composition in liquid (calculation)		
		Experiment	Calculation	Au/at.%	Ge/at.%	Ni/at.%
$L + \gamma Ni_3Ge \leftrightarrow \beta Ni_3Ge + \delta Ni_5Ge_2$	U_1	–	1,102	0.6	28.9	70.5
$L + \delta Ni_5Ge_2 \leftrightarrow Ni_5Ge_3 + \beta Ni_3Ge$	U_2	–	1,097	1.3	28.8	69.9
$L + fcc \leftrightarrow fcc + \beta Ni_3Ge$	U_3	921	937	43	8.7	48.3
$L + \beta Ni_3Ge \leftrightarrow fcc + Ni_5Ge_3$	U_4	904	889	55.7	15.2	29.1
$L + Ni_5Ge_3 \leftrightarrow NiGe + fcc$	U_5	549	497	74.5	24.0	1.5
$L \leftrightarrow Ge + NiGe + fcc$	E_1	362	357	70.2	29.6	0.2

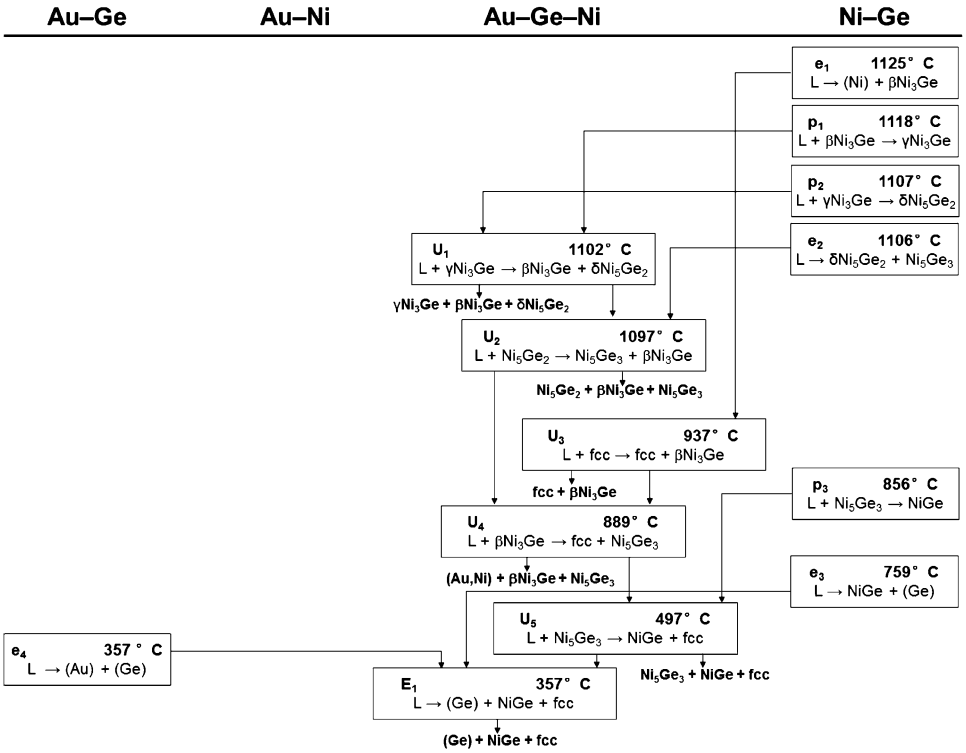

Fig. 10 Reaction scheme of the Au–Ge–Ni ternary system

Sn, Bi, Al, In, Ag, and Au. Samples after homogenization heat treatment at 325 °C for 648 h were used in the DSC experiments. The samples were polished and cleaned just before being measured in order to improve thermal contact and to avoid spurious or shifted transition peaks due to oxidation. Before each experiment, the DSC cell was evacuated three times and refilled with high-purity argon. Measurements were performed under a continuous flow of argon at a scanning rate of 10 °C/min (heating and cooling) and 5 °C/min (heating and cooling), separately. For each sample two heating/cooling cycles were performed.

The as-cast samples, annealed samples, and the samples after DSC measurements were then examined by SEM, XRD, and EPMA. XRD measurements were performed on a Panalytical X'Pert Pro X-ray diffractometer using Cu-Kα_1 radiation (40 kV, 40 mA) filtered with a Ge(111)-crystal monochromator at room temperature. The scanning range was $10° < 2\theta < 100°$ with a step size of 0.017° and a scan speed of 0.027°/s.

The compositions of the coexisting phases of each sample were determined by EPMA using a JEOL JXA8800 microanalyzer with an acceleration voltage of 30 kV and a probe current of 4×10^{-8} A. Pure element standards provided by JEOL were used for calibration. The measurements have a relative accuracy of about 1 %.

Acknowledgments This work was financially supported by the Swiss State Secretariat for Education and Research (SBF No. C08.0031) within the European COST action MP0602 on high temperature lead-free solder materials as well as by the Swiss National Science Foundation (SNSF no. 200021_134575/1).

References

1. Kang N, Na HS, Kim SJ, Kang CY (2009) J Alloy Compd 467:246
2. Kim SJ, Kim K-S, Kim S-S, Suganuma K (2009) J Electron Mater 38:266
3. Fima P, Gasior W, Sypien A, Moser Z (2010) J Mater Sci 45:4339
4. Schoeller H, Bansal S, Knobloch A, Shaddock D, Cho J (2009) J Electron Mater 38:802
5. Park J-H, Lee J-H, Kim Y-S (2002) J Electron Mater 31:1175
6. Toshio T, Satoru K, Masanori K, Noriharu K, Katsuhiko S (2005) Mater Trans 46:1825
7. Wang Q, Choa S-H, Kim W, Hwang J, Ham S, Moon C (2006) J Electron Mater 35:425
8. Massalski B (1990) Binary alloy phase diagrams. ASM, Metals Park
9. Chidambaram V, Hald J, Hattel J (2009) Microelectron Reliab 49:323
10. Chidambaram V, Hald J, Hattel J (2010) J Alloy Compd 490:170
11. Leinenbach C, Valenza F, Giuranno D, Elsener HR, Jin S, Novakovic R (2011) J Electron Mater 40:1533
12. Lang FQ, Yamaguchi H, Ohashi H, Sato H (2011) J Electron Mater 40:1563
13. Rai AK, Bhattacharya RS, Park YS (1984) Thin Solid Films 114:379
14. Piotrowska A, Guivarch A, Pelous G (1983) Solid State Electron 26:179
15. Jaffee RI, Gonser BW (1946) Trans Am Inst Min Met Eng 166:436
16. Christou A (1979) Solid State Electron 22:141
17. Kaufman L, Bernstein H (1970) Computer calculation of phase diagrams. Academic, New York
18. Wang J, Leinenbach C, Roth M (2009) J Alloy Compd 48:1830
19. Wang JH, Lu X-G, Sundman B, Su XP (2005) CALPHAD 29:263
20. Jin S, Leinenbach C, Wang J, Duarte LI, Delsante S, Borzone G, Scott A, Watson A (2012) CALPHAD (accepted)
21. Dinsdale AT (1991) CALPHAD 15:317
22. Redlich O, Kister AT (1948) Ind Eng Chem 40:345
23. Jansson B (1984) Tricta-Mac-0234. Royal Institute of Technology, Stockholm
24. Sundman B, Jansson B, Andersson JO (1985) CALPHAD 9:153